Article

Selective Methanol Carbonylation to Acetic Acid on Heterogeneous Atomically Dispersed ReO4/SiO2 Catalysts

Ji Qi, Jordan Finzel, Hossein Robatjazi, Mingjie Xu, Adam S. Hoffman, Simon R. Bare, Xiaoqing Pan, and Phillip Christopher

J. Am. Chem. Soc., **Just Accepted Manuscript** • DOI: 10.1021/jacs.0c05026 • Publication Date (Web): 21 Jul 2020

Selective Methanol Carbonylation to Acetic Acid on Heterogeneous Atomically Dispersed ReO_4/SiO_2 Catalysts

Ji Qi[1], Jordan Finzel[1], Hossein Robatjazi[1], Mingjie Xu[2,3,4], Adam S. Hoffman[5], Simon R. Bare[5], Xiaoqing Pan[2,3,4], Phillip Christopher[1*]

1. Department of Chemical Engineering, University of California, Santa Barbara, Santa Barbara, California 93117, United States.
2. Department of Materials Science and Engineering, 3. Department of Physics and Astronomy, 4. Irvine Materials Research Institute (IMRI), University of California Irvine, Irvine, California 92697, United States.
5. Stanford Synchrotron Radiation Light Source, SLAC National Accelerator Laboratory, Menlo Park, California 94025, United States

*Corresponding Author Email: pchristopher@ucsb.edu

Abstract

Methanol carbonylation to acetic acid (AA) is a large-scale commodity chemical production process that requires homogeneous liquid-phase organometallic catalysts with corrosive halide-based co-catalysts to achieve high selectivity and activity. Here we demonstrate a heterogeneous catalyst based on atomically dispersed rhenium (ReO_4) active sites on an inert support (SiO_2) for the halide-free, gas phase carbonylation of methanol to AA. Atomically dispersed ReO_4 species and nanometer sized ReO_x clusters were deposited on a high surface area (700 m^2/g) inert SiO_2 using triethanolamine as a dispersion promoter and characterized using aberration corrected scanning transmission electron microscopy (AC-STEM), UV-Vis spectroscopy and X-ray absorption spectroscopy (XAS). Reactivity measurements at atmospheric pressure with 30 mbar of methanol and CO (1:1 molar ratio) showed that bulk Re_2O_7 and ReO_x clusters on SiO_2 (formed at > 10 wt.%) were selective for dimethyl ether formation, while atomically dispersed ReO_4 on SiO_2 (formed at < 10 wt.%) exhibited stable (for 60 hours) > 93% selectivity to AA with single pass conversion > 60%. Kinetic analysis, *in-situ* FTIR and *in-situ* XAS measurements suggest that the AA formation mechanism involves methanol activation on ReO_4, followed by CO insertion into the terminal methyl species. Further, by introducing ~0.2 wt.% of atomically dispersed Rh to 10 wt.% atomically dispersed ReO_4 on SiO_2 > 96% selectivity toward AA production at volumetric reaction rates comparable to homogeneous processes were observed. This work introduces a new

class of promising heterogenous catalysts based on atomically dispersed ReO_4 on inert supports for alcohol carbonylation.

Keywords

single atom catalysts, atomically dispersed catalysts, methanol carbonylation, acid catalyst, acetic acid, Rhenium

1. Introduction

Acetic acid (AA) is a large-scale chemical used in the synthesis of vinyl acetate monomer, as well as many other commodity products.[1] Currently, a majority of the ~15 million tons of AA produced annually is synthesized through the carbonylation of methanol.[1,2] The Monsanto and Cavita processes are the primary commercialized routes for methanol carbonylation, which use Rh and Ru promoted Ir homogeneous catalysts, respectively, and operate under relatively mild conditions (180–220 °C, 2–4 MPa).[3,4] Despite being effective and selective, these commercial processes suffer from economic and environmental drawbacks. The former is due to the separation costs to recover the precious metal catalysts from liquid phase processes, whereas the latter is related to the essential role of hydroiodic acid that participates in the catalytic cycle.[5] Therefore, it is desirable to consider heterogeneous catalytic processes that rival homogeneous processes in terms of volumetric rates and selectivity, while simultaneously removing the need for reactive halogens.

Supported transition metal heterogenous catalysts have shown promise for methanol carbonylation.[2,6] However, most processes still rely on halide additives, and/or the reported reactivity, selectivity or stability are lower than existing homogeneous processes.[7,8] For example, atomically dispersed Iridium (Ir) on active carbon (AC) was shown to have comparable reactivity and selectivity to that of the analogous homogeneous catalyst, but its rapid deactivation precludes industrial viability.[9,10] Co-deposition of Lanthanum (La) resulted in a three-fold increase in reactivity compared to Ir/AC with an acetyl selectivity of 99% that remained stable for more than 1 month.[11,12] Analogously, atomically dispersed Rhodium (Rh) on porous organic polymers (POPs) has also shown good performance for methanol carbonylation, with catalyst stability for 400 hours on stream.[13–15] These heterogeneous catalytic processes still use halides and water, which minimizes the potential benefit over the already commercialized homogeneous processes.

By contrast, halide-free methanol carbonylation has been successfully demonstrated in the gas phase using 8-membered rings of mordenite (MOR) zeolites.[16–18] The strong acid sites in zeolites promote the primary reaction pathway of methanol coupling to produce dimethyl ether (DME), which then undergoes carbonylation to produce methyl acetate (MA). AA can then be produced in a second step involving the hydrolysis of MA back to methanol and AA, although this requires an additional water feed and a two reactor process.[19,20] Alternatively, by modifying zeolites with Cu species and operating with high (>50) CO:MeOH feed ratios, DME formation was suppressed, resulting in high AA selectivity in one step.[5,21] The requirement of either a two-step process or operation at very high CO:MeOH feed ratios limits the advantage of the gas phase zeolite-based AA production approaches. Hence, it remains a challenge to design catalysts that enable selective methanol carbonylation to AA in a gas-phase, iodide free heterogeneous catalytic process while operating close to stoichiometric CO:MeOH feed ratio.

Recent work on Al site pairing in zeolites and Na modification of ZrO_2-based catalysts demonstrated that decreased rates of DME formation in gas phase methanol feeds correlated with spatially separating acidic methanol adsorption and activation sites.[22–24] We hypothesized that isolated acidic sites on an inert support could minimize the on surface coupling of methanol species, suppressing DME formation and thereby promoting the selectivity toward AA through the carbonylation of surface methoxy species.

Here we demonstrate a heterogeneous catalyst based on atomically dispersed rhenium (ReO_4) active sites on an inert support (SiO_2) for stable halide-free, gas phase carbonylation of methanol to AA. Atomically dispersed ReO_4 species and ReO_x clusters were deposited on mesoporous high surface area (700 m^2/g) inert SiO_2 using triethanolamine as a dispersion promoter and stabilizer.[25] ReO_x structures were characterized by aberration corrected scanning transmission electron Microscopy (AC-STEM), UV-Vis spectroscopy and X-Ray absorption spectroscopy (XAS). In methanol carbonylation reaction measurements, atomically dispersed ReO_4 species (formed at < 10 wt.%) were found to exhibit stable > 93% selectivity to AA, while ReO_x clusters (formed at > 10 wt.%) were primarily selective for DME formation. Kinetic analysis, *in-situ* FTIR and *in-situ* XAS suggest that the reaction mechanism involves methanol activation on Lewis acidic ReO_4 sites, followed by CO insertion into the terminal methyl species.[26,27] Further, the addition of ~0.2 wt.% of atomically dispersed Rh to 10 wt.% atomically dispersed ReO_4 on SiO_2 increased AA

selectivity to more than 96%, resulting in volumetric AA production rates comparable to homogeneous processes. This work introduces a new class of promising heterogenous catalysts consisting of atomically dispersed ReO_4 on inert supports for gas phase, halide-free selective alcohol carbonylation.

2. Experimental Methods

2.1. Catalyst Preparation

Re catalysts were prepared by introducing water-soluble organics to induce complex formation with metal ions,[25] which may enhance the affinity between the supports and metal ions. Triethanolamine (TEA) (Sigma-Aldrich, 90278) was chosen, because amino groups can coordinate with metals and the hydroxyl groups can coordinate with the oxide support, which leads to metal anchoring on the oxide support. Mesoporous SBA-15 with 4 nm pore size (Sigma-Aldrich, 7631-86-9) was used as the support and perrhenic acid solutions ($HReO_4$) (Sigma-Aldrich, 75-80 wt.% in H_2O) were used as Re precursors. SBA-15 was chosen due to its high surface area (around 700 m^2/g) and chemical inertness. For the deposition of ReO_x species, appropriate amounts of Re precursor were dissolved in 10 mL of high-performance liquid chromatography (HPLC) grade water (J.T. Baker, JT4218-3) and the desired amounts of TEA (TEA:Re molar ratio of 8:1) were added into the solution under magnetic stirring for 30 min to ensure the solution was well mixed. The Re precursor solution was injected via syringe pump (5 mL/hr) into a 100 mL suspension of the SBA-15 support under magnetic stirring. After mixing for 12 hours at room temperature, the solution was dried at 80 °C using a rotary evaporator. For the synthesis of atomically dispersed Rh-ReO_4 pair sites on SiO_2, appropriate amounts of $HReO_4$ were dissolved in 10 mL of HPLC grade water and the desired amounts of TEA (TEA:Re molar ratio of 8:1) was added into the solution under magnetic stirring for 30 min to ensure the solution was well mixed, following which appropriate amounts of rhodium(III) chloride (Sigma-Aldrich, 307866) were added into the solution and stirred for another 30 minutes. The precursor solution was injected via syringe pump (5 mL/hr) into a 100 mL suspension of the SBA-15 support under magnetic stirring. After mixing for 12 hours at room temperature, the solution was dried at 80 °C using a rotary evaporator. The prepared catalysts were calcined at 450 °C for 4 hours under dry air prior to characterization and reactivity measurements.

Bulk Re_2O_7 (Sigma-Aldrich, 1314-68-7), which was used as a benchmark for the behavior of extended ReO_x domains, was physically mixed with SBA-15 prior to use.

2.2. Catalyst Characterization

2.2.1. Ultraviolet-visible diffuse reflectance spectroscopy

Ultraviolet-visible (UV–vis) diffuse reflectance spectroscopy was used to characterize the structure of ReO_x species on the SiO_2 support. Spectra were obtained using dehydrated MgO as a reference with a Thermo Scientific Evolution 300 UV–Vis spectrometer equipped with a Harrick Scientific Praying Mantis diffuse reflectance accessory. Samples were lightly ground using a mortar and a pestle before measurements following *in-situ* oxidation (O_2, 350 °C, 1 hour) and reaction conditions (30 mbar methanol and 30 mbar CO at 250 °C). Calculation of the onset of photon absorption induced by ligand to metal charge transfer (LMCT) was described previously.[28,29] For comparison, we obtained the LMCT onsets for $KReO_4$ and Re_2O_7, representing isolated ReO_4 and bulk ReO_x species, respectively.

2.2.2. X-ray absorption spectroscopy (XAS)

XAS at the Re L_3 edge (10535 eV) was executed on beamlines 4-1 and 9-3 at the Stanford Synchrotron Radiation Lightsource at the SLAC National Laboratory using a Si(220) double crystal monochromator. Spectra of Re reference compounds were collected by pressing finely ground powders into self-supporting pellets, while Re metal powder was smeared as a thin film on Kapton tape. In a typical experiment, 30 mg of catalyst was crushed, sieved (80-120 mesh), and loaded into a 1 cm catalyst bed in a 3 mm quartz tube flow-through reactor held perpendicular to the X-ray source.[30] Samples were diluted with mesoporous silica (MCM-41) to have an absorption length of 2.0 with a fractional absorbance of Re of about 0.2. A W foil was scanned simultaneously for energy calibration. *In-situ* extended X-ray absorption fine structure (EXAFS) measurements, consisting of 9-16 scans were collected at 50 °C following exposure to oxidizing (20% O_2/He, 350 °C, 1 hour) or reaction conditions (150 mbar methanol and 200 mbar CO in He, 250 °C, 1 hour).

The raw data were processed using the Athena interface of Demeter software package.[31] Spectra were energy calibrated, merged, and normalized. The EXAFS were extracted in k-space and Fourier transformed using the k^2-weighted EXAFS function (k=3.9-14) to amplify oscillations at high k-values. EXAFS fitting was carried out over the R range (1-2.2 Å) taking into account k^1-,

k^2-, and k^3-weighting using the Artemis interface of Demeter. Phase shifts and amplitude for relevant backscattering paths were calculated using FEFF6.[32] S_o^2 was determined to be 0.73 +/- 0.04 by fitting the Re metal standard (Figure S1). A multiple data set fit was performed for the 5, 10, and 20 wt.% Re loading samples simultaneously to minimize errors. Spectra were fit with two Re-O scattering paths derived from the crystal structure of tetrahedral Re in Re_2O_7 (mp-1016092). Coordination numbers to the short (double bonded) Re=O scattering path and long (single bonded) Re-O scattering path were fixed at 3 and 1 respectively, consistent with previous EXAFS treatment of similar samples, and the +7 Re oxidation state inferred from X-ray absorption near edge structure (XANES) measurements.[33,34]

2.2.3. High-angle annular dark field-scanning transmission electron microscopy (HAADF-STEM)

Atomic resolution high-angle annular dark field scanning transmission electron microscopy (HAADF-STEM) imaging was performed on a JEOL Grand ARM300CF microscope with double aberration correctors at 300 kV. Images were collected after *ex-situ* calcination of samples at 450 ℃ using a convergence semiangle of 22 mrad, and inner- and outer-collection angles of 83 and 165 mrad, respectively. A beam current of 11 pA was used with pixel time of 4 μs.

2.2.4. Temperature-programmed desorption of ammonia (NH_3-TPD)

NH_3-TPD measurements were performed on a Micromeritics AutoChem 2920 instrument. In a typical experiment, 0.15 g of catalyst was loaded into a U-shaped, flow-thru, quartz sample tube. Prior to measurements, the catalyst was pretreated in O_2 (30 cm^3 /min) at 350 °C for 1 h to remove adsorbed water. A mixture of 10% NH_3/90% helium was flown over the catalyst (30 cm^3 /min) at 50 °C for 1 h. Then the sample was flushed with pure helium (30 cm^3 /min) at 50 °C for 1 h. The TPD measurements were carried out in the range 100− 350 °C at a heating rate of 10 °C/min. NH_3 concentration in the effluent was monitored with a gold-plated filament thermal conductivity detector. The amount of desorbed NH_3 was determined based on the calibrated area under the desorption curve.

2.2.5. X-ray photoelectron spectroscopy (XPS)

High-resolution XPS measurements were performed on an Escalab Xi+ (ThermoFisher) XPS microprobe equipped with a monochromatic Al anode X-ray source. The pressure in the XPS

chamber was maintained below 1×10^{-9} torr during the acquisition process. XPS measurements were performed using the vacuum/inert transfer vessel with the use of glove box for the sample preparation and transfer, to enable analysis after pre-treatment without exposure to atmosphere.

2.2.6. Fourier Transform Infrared Spectroscopy (FTIR)

Catalysts were loaded into a Harrick Praying Mantis reaction chamber with ZnSe windows mounted inside a Thermo Scientific Praying Mantis diffuse reflectance adapter set inside a Thermo Scientific Nicolet iS10 Fourier transform infrared spectroscopy (FTIR) spectrometer. All gases were passed across an isopropyl alcohol/liquid nitrogen cold trap and a glass trap filled with Drierite desiccant to remove trace moisture. Before characterization, catalysts were pretreated via *in-situ* oxidation at 350 °C for 1 hour under O_2 flow, and a background spectrum was taken before CO and methanol introduction. The CO partial pressure was kept as 30 mbar, and methanol partial pressure was chosen as 42, 105 and 150 mbar with helium as a carrier gas. The spectra were collected under methanol and CO. In all measurements, spectra were obtained by averaging 32 sequentially collected scans at a resolution of 4 cm^{-1}.

2.3. Reactivity and kinetic measurements

Catalytic activity for methanol carbonylation was evaluated in a fixed-bed quartz reactor in the temperature range of 220-280 °C operating at atmospheric pressure. All gas flows were controlled by mass flow controllers (Teledyne Hastings) and an in-line bubbler, or syringe pump, was used to deliver methanol (Fisher Scientific, HPLC Grade, LOT: 177964) to the catalyst. Helium (Airgas, UHP, 99.999%) was used to bubble methanol and used as a diluent to control reactant partial pressures. The reaction effluent was quantified with online mass spectrometry (HALO 201, Hiden Analytical Inc.) and gas chromatography, which were independently calibrated. For online mass spectrometry the following m/z values were used to detect each product: m/z = 28 for CO, m/z = 31 for methanol, m/z = 45 for dimethyl ether (DME), m/z = 60 for acetic acid, and m/z=74 for methyl acetate. The concentrations were calibrated to the signal intensity at each mass and helium was used as an internal standard. The mass spec results were compared to calibrated analysis via gas chromatography, which showed quantitative agreement and the ability to close mass balances within ~5% under all explored conditions (selected mass balances over a range of conditions are shown in Table S1-3).

Prior to reactivity measurements, catalysts were pre-treated by oxidation at 350 °C for 1 hour with pure O_2 at 50 mL min^{-1}, followed by measurements at varying temperatures. The system was maintained for 2 h at each temperature to ensure steady state was achieved. Different Re weight loading catalysts were tested with 1, 5, 10 and 20 wt.% Re/SiO_2. During kinetic measurements, the total Re weight loading in the reactor was kept constant by using different weights of catalysts and diluent SBA-15. Additionally, SiO_2 gel was added to minimize the pressure drop (Table S4). When analyzing the influence of methanol conversion on selectivity over the 10 wt.% Re/SiO_2 catalyst, the amount of both Re and SBA-15 were varied, while the amount of diluent SiO_2 was kept constant (Table S5). The stability measurement was executed with 600 mg of 10 wt.% Re/SiO_2 diluted in 600 mg SiO_2 at 280 °C.

For methanol and CO pressure-dependent experiments, 10 wt.% Re/SiO_2 was pretreated by oxidation at 350°C for 1 h. After the pretreatment, while maintaining a constant temperature of 280°C and methanol partial pressure at 30 mbar, the CO partial pressure was varied from 200 mbar to 600 mbar with Ar as a diluent. Alternatively, while maintaining a constant temperature of 280°C and CO partial pressure at 30 mbar, the methanol partial pressure was varied from 30 mbar to 330 mbar and Ar acted as a diluent. The reaction system was held at each condition for 2 h to ensure steady state conditions.

3. Results

3.1 Characterization of ReO_x structure

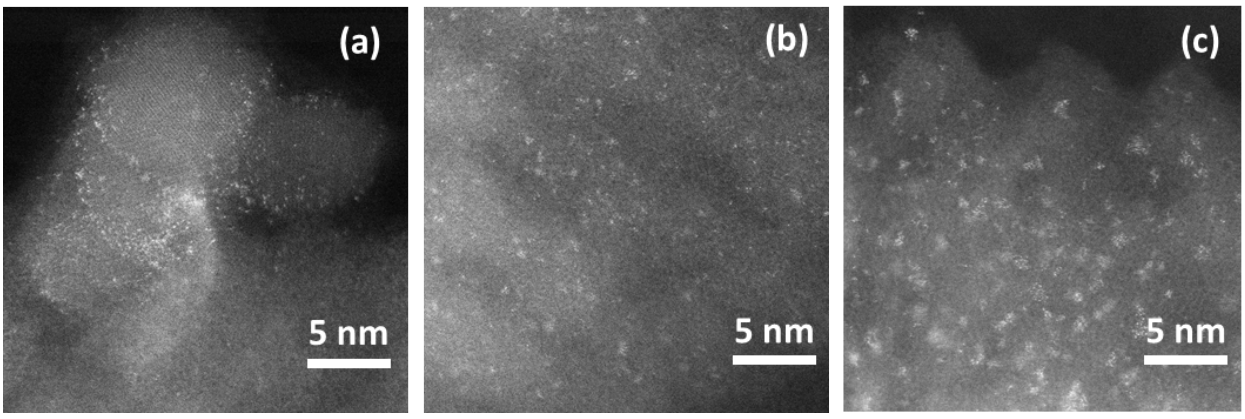

Figure 1. Representative HAADF-STEM images of (a) 5 wt% Re/SiO_2, (b) 10 wt% Re/SiO_2 and (c) 20 wt% Re/SiO_2. Samples were pretreated via calcination at 450 °C for 4h in dry air prior to measurements.

Re/SiO_2 catalysts at various Re weight loadings (1, 5, 10, and 20%) were synthesized through impregnation of aqueous perrhenate ($HReO_4$) with the addition of 8:1 molar ratio of triethanolamine (TEA) to promote Re dispersion.[25] HAADF-STEM images of the calcined (450 °C, dry air) samples are presented in Figure 1(a-c), where the higher atomic number of Re as compared to Si allows identification of Re domains via increased scattering of the electron beam. While atomically dispersed Re species were primarily observed for the 5 wt% Re sample, an increase in the density and existance of Re clusters was observed with increasing Re loading to 10 and 20 wt.%. However, the fraction of Re clusters in each sample is likely an over estimation of the as-prepared state due to the electron beam induced coalescense during image acquisition.[35] Previoius analysis of WO_x speceis on ZrO_x noted that analysis by STEM imaging suggested higher concentrations of WO_x clusters than atomically dispersed species as compared to correlated spectrscopic measurements.[36]

To provide sample-averaged information on the ReO_x structure without influence of the elctron beam, UV-vis and XAS were performed. *In-situ* UV-Vis spectroscopy measurements of the edge energy (E_g) for the LMCT electronic transition were executed under an oxidative environment, and reaction conditions. E_g provides useful information regarding the electronic structure of the ReO_x species, which is sensitive to the ReO_x domain size and structure (moving from discrete electronic structure of monomeric species to bands existing in bulk structures).[29] Figure 2a shows a decrease in E_g with increasing Re weight loading from ~4.45 eV for 1 and 5 wt% Re to ~4.1 eV for 20 wt% Re following *in-situ* calcination in O_2 at 350 °C and exposure to reaction conditions at 250 °C. A comparison of the E_g values to that of control samples, dispersed ($KReO_4$, E_g = 4.1 eV) and bulk (Re_2O_7, E_g = 2.8 eV) ReO_x species, suggests that at lower Re weight loadings (1, 5 and 10 wt%) ReO_x exists predominantly in the form of atomically dispersed species, while ReO_x clusters are present at higher Re weight loadings and their size increases with increasing Re loading. The similar E_g following calcination and reaction conditions suggests that ReO_x domains remain stable under reaction conditions. This is in contrast to a previous report in which ReO_x on SiO_2 was unstable after 2 hours during 2-butanol dehydration,[37] suggesting that the use of TEA during synthesis promotes the stability of a highly dispersed ReO_x species on SiO_2.

XAS was used to further characterize the oxidation state and structure of ReO_x species on the support. Re/SiO_2 samples of various weight loadings showed nearly identical XANES spectra

following oxidation (Figure 2b), with edge energies correlating to Re in +7 oxidation state (Figure S2), which was also comfirmed by XPS (Figure S3). EXAFS spectra were fit with a proposed ReO_4 model that is consistent with the Re +7 oxidation state observed from XANES, in which Re makes a single bond to the support via oxygen (Re-O 1.77 ± 0.04 Å), and is coordinated to three additional Re=O double bonds (Re-O 1.69 ± 0.01 Å). The fit yielded a good match to the measured EXAFS spectrum for the 5 wt% Re sample (Figure 2c). The EXAFS data and fit (Figure S4, fit parameters in Table S6) are also in agreement with previously reported structures of atomically dispersed ReO_4.[33,34] Notably, the EXAFS data for the 5, 10 and 20 wt% Re samples did not vary considerably (Figure S4), suggesting that this sample averaged technique may not be able to unambiguously identify small, sub-nanometer ReO_x clusters within a sample containing atomically dispersed ReO_4 species.[38] This is not unsuspected, as even bulk crystalline oligomeric Re species (Re_2O_7) show Re-O-Re scattering at long bond lengths (Figure S5), which is thus more sensitive to destructive interference from competing multiple scattering paths. Therefore EXAFS likely, in contrast to STEM, underestimates the existence of ReO_x clusters present. Based on a combination of STEM, UV-Vis and XAS, it is concluded that ReO_x was primarily atomically dispersed as ReO_4 species for 1 and 5 wt% Re, a mix of atomically dispersed ReO_4 and small ReO_x clusters for 10 wt% Re, and primarily in the form of ReO_x clusters for 20 wt% Re.

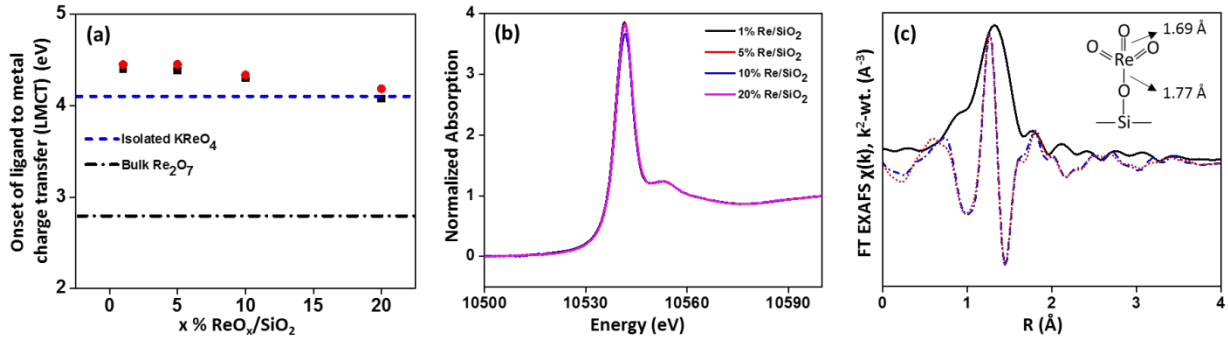

Figure 2. (a) Onset of LMCT of dehydrated Re/SiO_2 measured by *in-situ* UV−vis spectroscopy as a function of Re loading. Measurements were performed after catalysts were oxidized at 350 °C for 1h (red dots) and after the catalysts were exposed to 30 mbar methanol and 30 mbar CO at 250 °C for 1 hr (black dots). Measurements for the LMCT for reference compounds ($KReO_4$ and Re_2O_7) were included for comparison. (b) Re L_3-edge XANES spectra characterizing various Re weight loading samples after 1h oxidation in 20% O_2/He at 350 °C. The slightly lower absorbance for the 10 wt% Re sample is likely due to absorbance saturation by the detector. The edge energy was consistent with other samples supporting consistent +7 oxidation state for Re. (c) EXAFS of 5 wt% Re/SiO_2 after 1h

oxidation in 20% O_2/He at 350 °C. The magnitude and imaginary portion of the Fourier transformed EXAFS are shown by the solid black and dashed blue lines, respectively while the fit to the imaginary portion is shown in red. The inset shows the model used to fit the EXAFS spectrum.

3.2 Influence of Re Structure on Methanol Carbonylation

On the basis of the UV-vis, STEM and XAS, the influence of ReO_x structure on reactivity and selectivity for methanol carbonylation was examined by comparing reactivity as a function of Re weight loading. Bulk Re_2O_7 was also used to calibrate the reactivity of extended ReO_x domains. Catalysts were pre-oxidized at 350 °C in O_2 before being exposed to a mixture of methanol and CO at a molar ratio of 1:1 (at 30 mbar of each) with a balance of helium at atmospheric pressure. The reaction was executed in the kinetically limited regime by keeping the methanol conversion below 10% (Figure S6). Arrhenius plots of the reactivity for AA and DME production as a function of Re loading are shown in Figure 3a and b with production rates normalized to the Re weight loading. The results for MA and formaldehyde production rates are provided in Figure S7. The bare SBA-15 support showed no measurable reactivity under these conditions.

For 1 and 5 wt% Re/SiO_2 catalysts, the AA and DME production rates were indistinguishable, showing 0.038 mmol s^{-1} g_{Re}^{-1} and 0.0005 mmol s^{-1} g_{Re}^{-1}, respectively, at 280 °C. For 10% Re/SiO_2, the AA production rate decreased slightly to 0.0285 mmol s^{-1} g_{Re}^{-1} at 280 °C and the DME production rate increased slightly to 0.0006 mmol s^{-1} g_{Re}^{-1}. However, increasing the Re loading to 20 wt% resulted in a 30-fold increase in the DME production rate at 280 °C, while the AA production rate decreased by 5-fold compared to that of the 1 and 5 wt% Re/SiO_2. Compared to the 20 wt.% Re sample at 280 °C, bulk Re_2O_7 showed a DME production rate of only two-fold higher and a 50% lower AA production rate. The similar reactivity of 20 wt.% Re/SiO_2 and Re_2O_7, and their stark difference to the behavior of samples with 10 wt.% Re or less, substantiate the use of Re weight loading variation for comparing the behavior of atomically dispersed ReO_4 and ReO_x clusters.

The measured apparent activation energies (E_{app}) for AA and DME formation were similar for 1 and 5 wt.% Re/SiO_2, showing E_{app} of ~130±30 kJ/mol and ~100±40 kJ/mol for AA and DME formation, respectively. On 10 wt.% Re/SiO_2 the E_{app} for AA and DME formation were 155±20 and 112±28 kJ/mol, respectively. The slight deviation of the E_{app} on 10 wt% Re/SiO_2 from 1 and 5 wt.% Re/SiO_2, suggests relatively consistent active site distributions with a small increase in

ReO_x cluster formation at the higher weight loading, in agreement with inferences from catalyst characterization. On the 20 wt.% Re/SiO_2 the E_{app} for AA and DME were much higher, 259±64 and 257±9 kJ/mol, respectively. Bulk Re_2O_7 exhibited E_{app} of 272±33 and 273±32 kJ/mol for the formation of AA and DME, respectively, which are statistically similar to the 20 wt.% Re/SiO_2 sample. We note that there is some apparent deviation from Arrhenius like behavior at lower temperatures in Figure 3a. This likely arises from the low analytical signals at these temperatures, rather than a true deviation from exponential behavior.

We hypothesize that differences in the measured E_{app} for AA and DME formation over atomically dispersed ReO_4 versus ReO_x clusters on SiO_2 and bulk Re_2O_7 derives from differences in acidity, as measured by NH_3 temperature programmed desorption shown in Figure S8 structure. Relationships between ReO_x weight loading on oxide supports, acid strength and reactivity have previously been observed.[28,39,40,41] Together with our results, this suggests that ReO_x domain size dictates acid strength.

The product formation rates and E_{app} on the 1, 5, and 10 wt.% Re/SiO_2 catalysts provide evidence that a consistent active site exists with a close to linear relationship between site density and reactivity. Previous work on Re species for olefin metathesis showed that not all the Re sites are active and the reactivity was not linearly related to weight loadings.[42–44] Thus, the reactivity results here suggest that either the majority of sites on Re/SiO_2 are active, or the same fraction of active sites are produced for different weight loadings.[45] Figure 3c shows the measured selectivity for AA production in the range of 220-280 °C, where samples at lower weight loadings (1%, 5% and 10 wt.% Re/SiO_2) exhibit an AA selectivity of ~93% at > 250 °C, whereas 20 wt% Re/SiO_2 and bulk Re_2O_7 exhibited AA selectivity < 20% across all temperatures. It is noted that at above 280 °C a significant increase in the rates of byproduct formation were observed, resulting in a decrease in AA selectivity.

Based on the characterization and methanol carbonylation reactivity results it can be concluded that atomically dispersed ReO_4 species on SiO_2 are selective for AA formation, whereas ReO_x clusters and bulk Re_2O_7 with stronger acid sites primarily drive DME production. This suggests that communicating acidic sites existing on the surface of ReO_x clusters facilitate the rate of methanol coupling to DME, as initially hypothesized.[46,47] This will be discussed further below. The DME carbonylation reaction was tested on 5 wt.% Re/SiO_2 using 30 mbar DME and 30 mbar

CO in the feed, Figure S9. The DME carbonylation reaction to MA proceeded with 12 times higher rate than methanol carbonylation to AA under identical conditions. This highlights the critical role of minimizing DME formation pathways for obtaining high selectivity to AA. We also note that water, which is a product during DME formation, may compete with other reaction intermediates at Lewis acid sites[26,48] and may poison active sites that contribute to the production of AA. The influence of water on AA formation will be analyzed in future work.

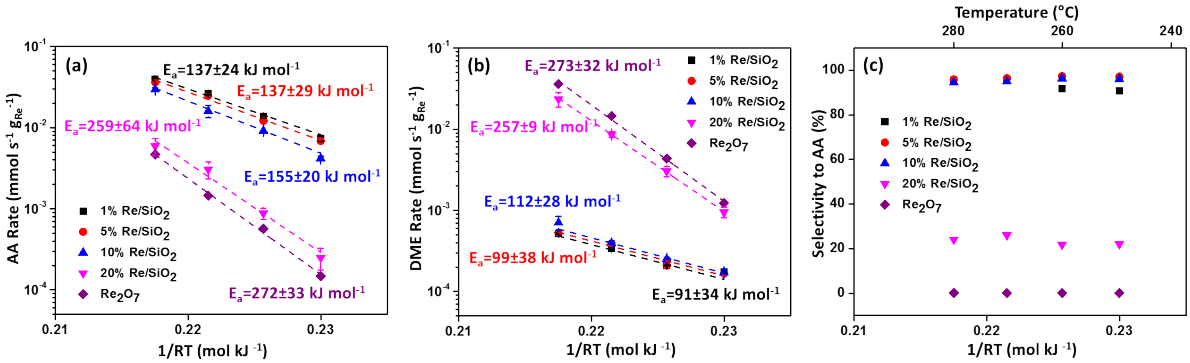

Figure 3. Arrhenius plots showing the (a) AA formation rate and (b) DME formation rate on a per-gram Re basis (mmol s^{-1} g_{Re}^{-1}). The error bars on each data point represent the standard deviation calculated from 2 independently run reactions. The error on E_{app} estimates is the 90% confidence interval of the fit. (c) AA selectivity during methanol carbonylation from 200 to 280 °C under 30 mbar methanol and CO (balance He).

We investigated the influence of methanol conversion on AA selectivity and catalyst stability for the 10 wt.% Re/SiO_2 catalyst, which exhibited the highest volumetric AA production rates still with good selectivity (Figure 4a). To analyze the influence of methanol conversion on selectivity, the loading of 10 wt.% Re/SiO_2 in the reactor was increased, while the amount of diluent SBA-15 was decreased such that the space velocity was identical in all experiments. Increasing the catalyst loading resulted in increasing methanol conversion to ~60%, which was limited from further increases based on the reactor size. The measured AA selectivity was independent of methanol conversion, showing ~93% selectivity for different methanol conversions (Figure 4b). Catalyst stability measurements were performed at 280 °C in 30 mbar of MeOH and CO with 600 mg of 10 wt.% Re/SiO_2 catalyst (the highest catalyst loading we used here). Figure 4c shows a stable ~60% methanol conversion and 93% AA selectivity over 60 hours on stream, suggesting that the atomically dispersed ReO_4 active sites on SiO_2 remain quite stable under the explored reaction conditions.

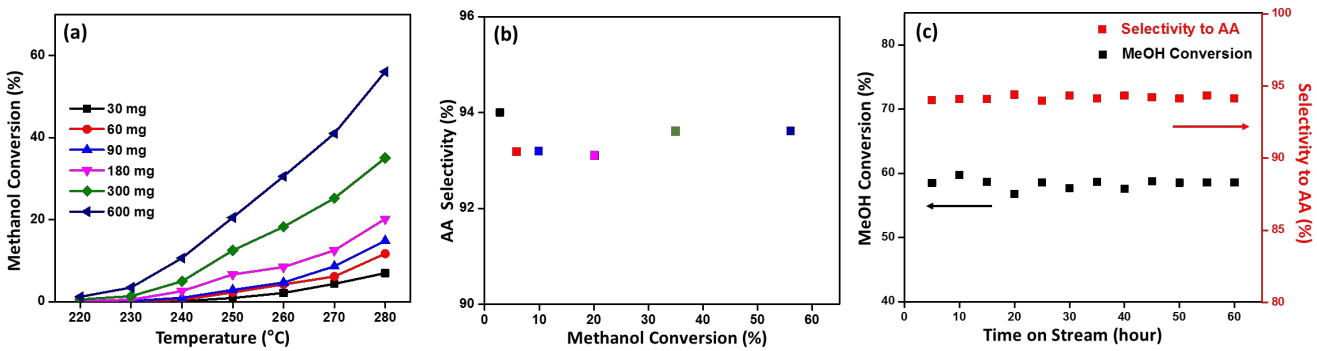

Figure 4. (a) Methanol conversion as a function of temperature for various amounts of 10 wt% Re/SiO_2 added to the reactor (balance was SiO_2 to give a total amount of material added to the reactor of ~1.2 g in all cases) at 30 mbar methanol and 30 mbar CO (with balance of He). (b) AA selectivity as function of methanol conversion measured at 280 °C from the data in (a). (c) Methanol conversion and AA selectivity as a function of time on stream with 600 mg of 10 wt% Re/SiO_2 catalyst at 280 °C with 30 mbar methanol and CO (balanced with He).

3.3 Reaction pathway for methanol carbonylation to AA on ReO_4/SiO_2

Mechanistic insights into the observed AA formation on atomically dispersed ReO_4 species and ReO_x clusters were developed by executing methanol carbonylation on 10 and 20 wt.% Re/SiO_2 at 280 °C with independently varied methanol and CO partial pressures in the range of 30 to 330 mbar and 200 to 600 mbar, respectively (Figure 5). Figure 5a shows that for 10 wt.% Re/SiO_2 (mostly atomically dispersed ReO_4) a first-order dependence of AA production on methanol partial pressure was observed in the range of 30-90 mbar, which transitioned to a zero-order dependence at higher methanol pressure. This indicates that methanol, or a methanol derived intermediate, is first-order in the rate determining step (RDS) and saturates the active site at methanol partial pressures > ~120 mbar. For 20 wt.% Re/SiO_2 that contained a mix of atomically dispersed ReO_4 and ReO_x clusters, a ~0.6 reaction order for methanol partial pressure in the AA production rate was observed from 30-85 mbar, with an apparent decrease in methanol reaction order at ~85 mbar, followed by a small increase in methanol reaction order up to ~120 mbar, and finally a reaction order of 0 above ~120 mbar. The distinct kinetic behavior of the two types of sites is consistent with the differences in E_{app} for AA formation observed in Figure 3 and may also be influenced by H_2O produced due to DME formation.

In contrast to methanol, the AA production rate exhibited nearly a first-order (0.8-0.9) dependence on CO partial pressure for both catalysts across a broad partial pressure range from 200 to 600

mbar CO (Figure 5b). This suggests that CO is involved in the RDS, and that CO does not exist as an adsorbed species at an appreciable coverage on the active site.[18,48,49]

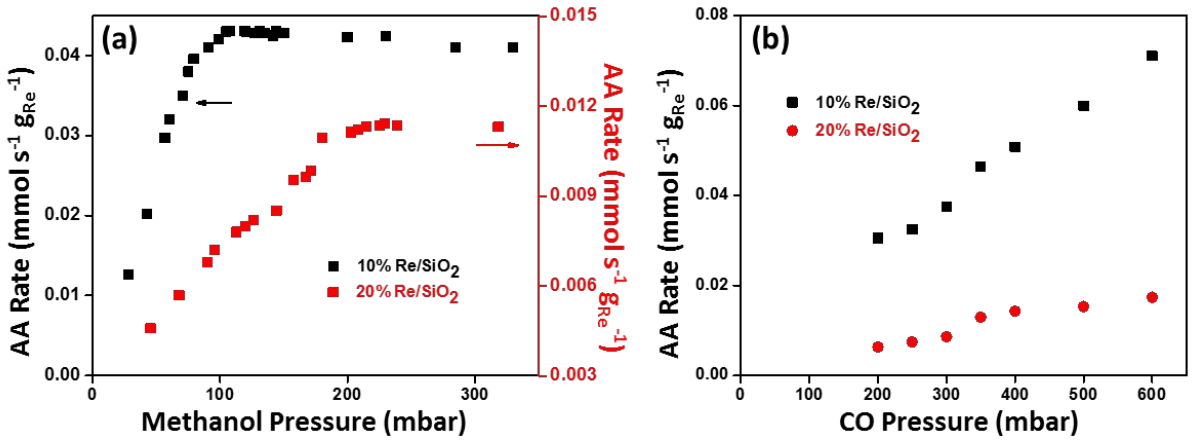

Figure 5. AA production rates as a function of (a) methanol partial pressure and (b) CO partial pressure over 10 wt% Re/SiO_2 and 20 wt% Re/SiO_2. In both sets of experiments, the non-varied reactant partial pressure was held constant at 30 mbar. Before reactivity experiments, the catalyst was oxidized at 350 °C for 1 h.

The nature of bound species during AA formation on atomically dispersed ReO_4 species was analyzed via *in-situ* FTIR measurements executed under varying methanol partial pressure (at a constant CO partial pressure of 30 mbar) at 280 °C on 5 wt.% Re/SiO_2 (Figure 6a). Independent of the methanol partial pressures, two strong bands at 2954 and 2854 cm^{-1} were observed that correspond to physiosorbed methanol on SiO_2, as they were also seen on pure SiO_2 (Figure S10).[50,51] Three bands at 2979, 2922 and 2822 cm^{-1} (marked with the dashed lines) were also observed. We assign the 2979 and 2922 cm^{-1} bands to the asymmetric and symmetric stretches of CH_3 in $-OCH_3$ bound to ReO_4, respectively, while 2822 cm^{-1} is assigned as the first overtone of the symmetric stretch.[52]

Alcohol activation on the homogeneous methyltrioxorhenium complex (MTO, CH_3ReO_3), in which Re exists in a +7 oxidation state, has been studied previously.[53–55] Based on theoretical analysis and isotopic labelling experiments it was proposed that dissociative alcohol adsorption occurs through proton transfer from the alcohol to an oxygen native of MTO, resulting in the coordination of -OR group to the Lewis acidic Re center, thus a maintained +7 oxidation state of Re. This is analogous to the mechanism for ethanol activation over Lewis acidic Al_2O_3 surfaces, where $-OCH_2CH_3$ coordinates to the Lewis acidic Al center, while the proton transfers to a neighboring oxygen.[56–60] Thus, it is hypothesized that methanol adsorption onto ReO_4 occurs

dissociatively at the O-H group, resulting in the formation of Re(-O-Si)(-OH)(=O)$_2$(-OCH$_3$), where Re remains in a +7 oxidation state.

With increasing methanol partial pressure in the feed from 42 mbar to 105 mbar an increase in the intensity of the bands assigned to -OCH$_3$ stretches were observed, indicating an increase in the coverage on ReO$_4$ sites. However, the -OCH$_3$ stretch intensities remained unchanged with further increase in the methanol partial pressure to 150 mbar, suggesting saturation of adsorption sites on ReO$_4$ species. The *in-situ* FTIR results are consistent with the kinetic measurements shown in Figure 5a, where a saturation in the methanol reaction order in AA formation rate correlates with a saturation in -OCH$_3$ adsorption sites. This suggests that the resting state or most abundant surface intermediate (MASI) for the ReO$_4$ species at methanol partial pressure > ~120 mbar is Re(-O-Si)(-OH)(=O)$_2$(-OCH$_3$), containing dissociatively adsorbed methanol.

The oxidation state of atomically dispersed ReO$_4$ species was probed with *in-situ* XANES measurements for pre-oxidized 5 wt.% Re/SiO$_2$ and under methanol carbonylation reaction conditions where kinetic measurements and *in-situ* FTIR suggest that ReO$_4$ species should be saturated with -OCH$_3$ (150 mbar methanol, 200 mbar CO and 250 °C). As observed in Figure 6b, the XANES region did not change due to exposure to reaction conditions suggesting that Re was in a +7 oxidation state in the most occupied state in the reaction cycle, consistent with the proposal above. While the XANES region of 5 wt.% Re/SiO$_2$ was indistinguishable comparing pre-oxidized and under reaction conditions, changes in the EXAFS region were observed (Figure 6c). The intensity of the scattering feature associated with scattering from oxygen in the first coordination shell of Re decreased under reaction conditions. These changes could be consistent with a decreased coordination number to shorter Re=O bonds and increased coordination to longer Re-O bonds that have weaker scattering intensity, (Figure S11).[53–55] We do not rule out the possibility of CO-induced restructuring of ReO$_x$ species. Additional quantitative analysis is beyond the scope of this work, but could provide further insights. The *in-situ* XANES and EXAFS under reaction conditions are consistent with the proposed MASI described above.

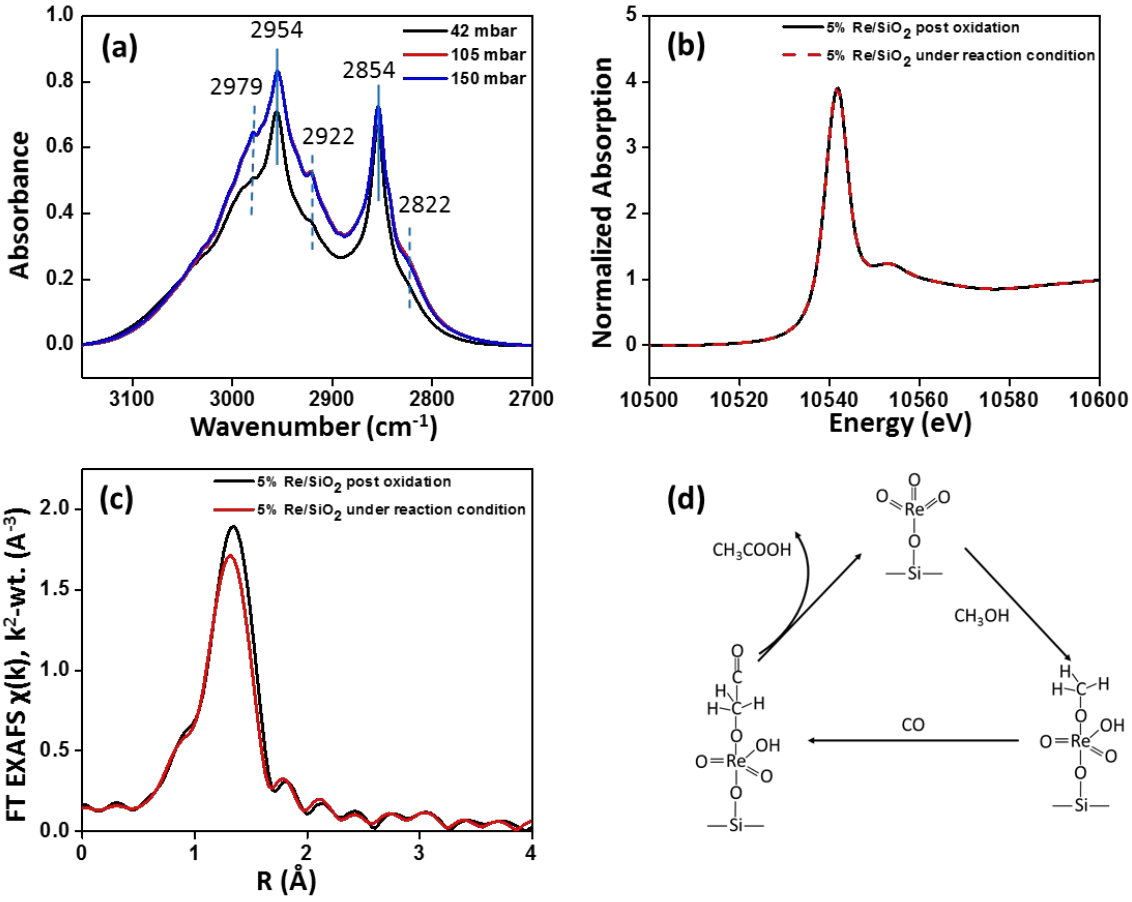

Figure 6. (a) *In situ* FTIR spectra for 5 wt% Re/SiO_2. The samples were oxidized at 350 °C for 1h before being exposed to 42, 105 and 150 mbar methanol with a CO partial pressure of 30 mbar (balanced by He). (b) Re L_3-edge XANES spectra collected under oxidation condition (under O_2 at 350 °C) and reaction condition (150 mbar methanol and 200 mbar CO diluted in He, 250 °C, 1 hour) for 5 wt% Re/SiO_2. (c) EXAFS spectra collected at 50 °C after 350 °C oxidation and 250 °C reaction condition for 5 wt% Re/SiO_2. (d) Proposed mechanism for AA formation on atomically dispersed ReO_4 species.

It is proposed that AA formation on atomically dispersed ReO_4 active sites on SiO_2 occurs through dissociative methanol adsorption to form $Re(\text{-}O\text{-}Si)(\text{-}OH)(=O)_2(\text{-}OCH_3)$, see Figure 6d. Based on the partial pressure dependent methanol reaction order for AA formation, *in-situ* FTIR and *in-situ* XAS it is proposed that this species is the MASI when the methanol partial pressure is > 120 mbar. Because the AA formation rate is first order in methanol and CO at lower methanol partial pressures, it is proposed that the RDS is CO insertion into the terminal CH_3 group of the $Re(\text{-}O\text{-}Si)(\text{-}OH)(=O)_2(\text{-}OCH_3)$ species. Typically, for methanol carbonylation on homogeneous Rh catalysts CO insertion is a migratory process into the M-C bond of $Rh\text{-}CH_3$ species.[4,61,62] However,

for the halide-free methanol carbonylation process in zeolites where an Al-O-CH_3 intermediate participates in the CO insertion reaction, extensive DFT calculations have shown that the energetically feasible pathway is CO insertion into the terminal CH_3.[26,49,63] Given the similar proposed M-O-CH_3 structure for ReO_4 active sites, it is hypothesized that a similar CO insertion into the carbon end of the bound -O-CH_3 species followed by the rearrangement to acetyl group occurs for ReO_4 active sites, although further analysis is needed to confirm this. Finally, it is proposed that the proton transfers back to form AA that desorbs, leaving ReO_4 intact, Figure 6c.

The rate law for AA formation within this mechanism can be written as (see SI for derivation):

$$\text{AA Production Rate} = \frac{k_2 K_1 P_{CO} P_{CH_3OH}}{1 + K_1 P_{CH_3OH}} \quad (1)$$

Where, K_1 is the equilibrium constant for dissociative methanol adsorption, and k_2 is the rate constant for the gas phase attack of CO on surface bound methoxy. At lower methanol partial pressure, vacant sites are abundant, and the denominator of the rate law is approximately equal to 1, thus, the rate law appears as a first-order with respect to methanol and CO partial pressures. In contrast, at higher methanol partial pressures, active sites are saturated with dissociatively adsorbed methanol and the denominator becomes $K_1 P_{CH3OH}$, which results in a zero-order dependence of AA formation on the methanol partial pressure.

3.4 Influence of ReO_x structure on DME formation.

There are two proposed reaction pathways for DME formation: (i) through the interaction of gas phase methanol with surface methoxy species (the dissociative mechanism),[26] and (ii) through the coupling of two adsorbed methanol species to produce DME (the associative mechanism).[22,64] In zeolites, the reaction pathways and rates of DME formation vary based on whether acid sites are isolated or paired.[24,46,47] Similar to recent analysis of the influence of acid site pairing in zeolites on the DME formation rate, we observed an order of magnitude increase in DME production rate comparing atomically dispersed ReO_4 and ReO_x clusters, where contiguous acidic sites likely exist on the cluster surfaces, Figure 3b.

On 10 wt% Re/SiO_2 the DME formation rate exhibited a second-order dependence on methanol up to ~100 mbar and a transition to a zero-order at higher partial pressures, Figure 7a. Conversely, on ReO_x clusters (20 wt% Re) the DME formation rate was inhibited at methanol partial pressures

> 85 mbar. The second order dependence on methanol partial pressure is consistent with the bimolecular reaction leading to DME formation. Inhibition of the DME formation rate at higher methanol pressures has recently been ascribed to the formation of supramonolayer coverages of methanol in the case of DME formation in small pore zeolites.[24] In this context, the data in Figure 7a suggests that ReO_x clusters can support supramonolayer methanol or methoxy coverage, which cannot occur on atomically dispersed ReO_4 active sites, although this requires further analysis.[24] Both catalysts exhibited a negative CO reaction order for DME formation, which suggests a competition between CO and methanol in reactions with adsorbed -OCH_3 species, Figure 7b.

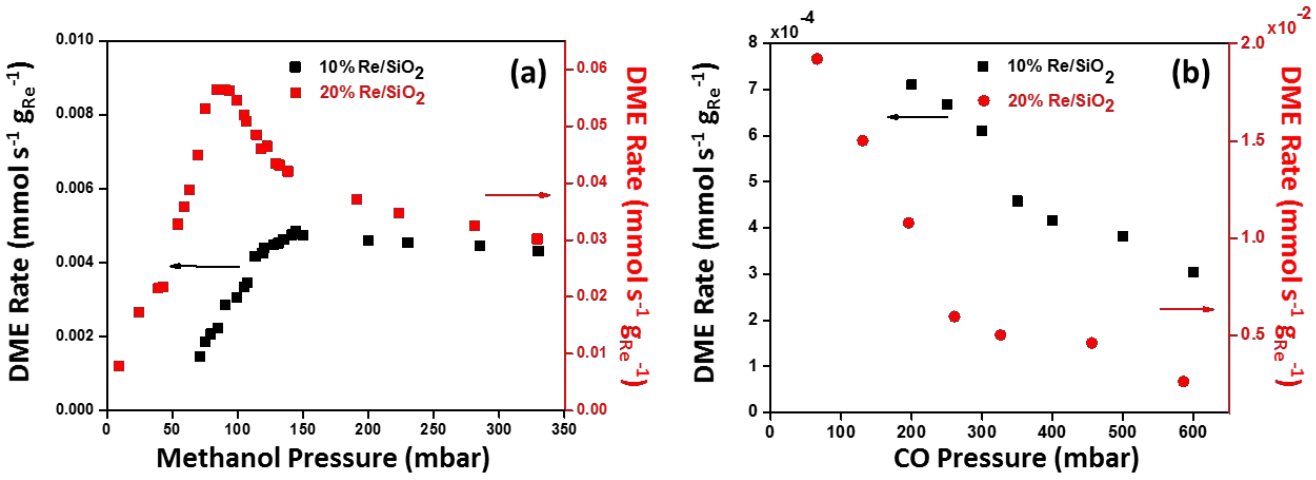

Figure 7. DME production rates as a function of (a) methanol partial pressure and (b) CO partial pressure over 10 wt.% Re/SiO_2 and 20 wt.% Re/SiO_2. In both sets of experiments, the non-varied reactant partial pressure was held constant at 30 mbar. Before reactivity experiments, the catalyst was oxidized at 350 °C for 1 h.

3.5 Promoting ReO_4/SiO_2 reactivity with atomically dispersed Rh

It was hypothesized from the kinetic data that critical features of the ReO_4/SiO_2 active site that enable high AA selectivity are (i) reduced rates of DME formation, which may result from the effective blocking of the associative DME formation pathway by the isolated active sites, and (ii) the ability of CO to outcompete methanol in the attack on the terminal CH_3 in bound -OCH_3 species.[26,27] We previously showed that atomically dispersed Rh can promote CO insertion into methoxy species bound to neighboring acidic sites on a ZrO_2 support.[22] Therefore, we postulated that the formation of Rh-ReO_x pair-sites on SiO_2 could further promote the AA production rate on atomically dispersed ReO_4 active sites. Atomically dispersed Rh-ReO_x pair-sites catalysts were prepared and characterized by CO probe molecule FTIR, as we recently reported on Al_2O_3.[65]

Figure 8a shows CO probe molecule FTIR spectra for 0.2 wt.% Rh/SiO_2 and 0.2 wt.% Rh/10 wt.% Re/SiO_2 at saturation coverage and room temperature. Two strong bands centered at 2091 and 2030 cm^{-1} were observed for 0.2 wt.% Rh/SiO_2, which are assigned to the symmetric and asymmetric stretches of the $Rh(CO)_2$ *gem*-dicarbonyl species, demonstrating the predominant existence of atomically dispersed Rh species.[66,67] Another CO stretch at 2107 cm^{-1} was observed, which has been assigned to an atomically dispersed Rh species that is simultaneously coordinated to CO and an additional O.[68] A blue-shift of ~6 cm^{-1} in the CO stretch frequency for $Rh(CO)_2$ species was observed comparing Rh/ReO_x-SiO_2 and Rh/SiO_2. The CO stretch frequency in $Rh(CO)_2$ depends on the supports ability to withdraw or donate charge to Rh. Thus, the blue shift is evidence that Lewis acidic ReO_x species reduced the charge transfer to CO species bound to Rh.[28,65,69] We recently correlated a similar blue shift in CO frequency with the formation of Rh-Re atomically dispersed pair sites on Al_2O_3 through correlation with HAADF-STEM imaging, providing confidence in the formation of Rh-Re atomically dispersed pair sites in the current catalyst. However, we note that the coordination environment in this interaction and its dependence on reaction conditions is yet to be unraveled.

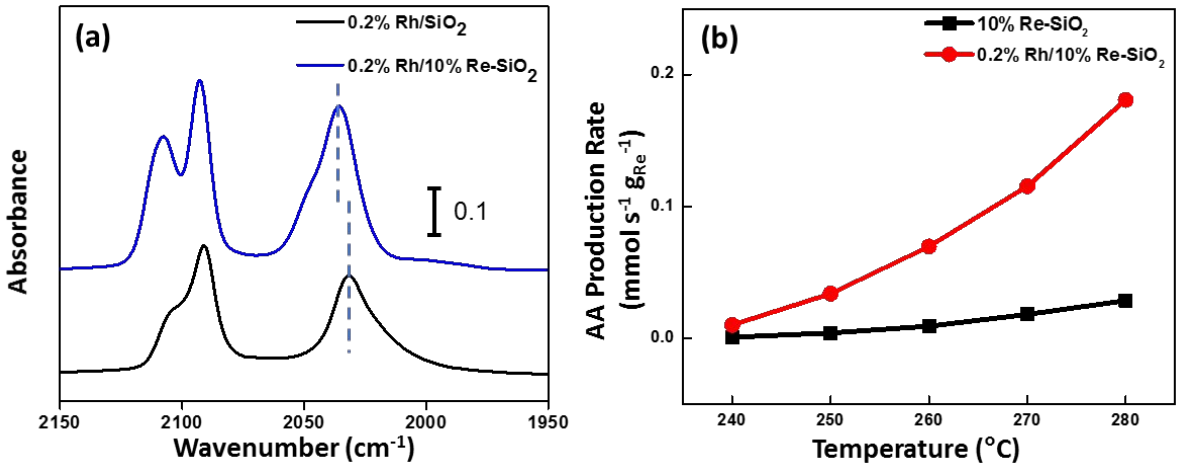

Figure 8. (a) CO probe molecule FTIR spectra of Rh/SiO_2 and Rh/ReO_x–SiO_2 catalysts. The catalysts were reduced at 250 °C under CO and spectra were collected under Ar. (b) AA production rate comparison between 10 wt.%Re/SiO_2 and 0.2 wt.% Rh/10 wt.% Re-SiO_2. The catalysts were oxidized at 350 °C for 1h before being exposed to the reaction condition (30 mbar methanol and CO).

Methanol carbonylation reactivity measurements at 30 mbar methanol and CO as a function of temperature are shown in Figure 8b for 10 wt.% Re/SiO_2 and 0.2 wt.% Rh/10 wt.% Re-SiO_2. This comparison showed an order of magnitude increase in the rate of AA formation, without promoting

DME formation (Figure S12), with the addition of 0.2 wt.% Rh. This results in an increase of AA selectivity to ~96%, even at the stoichiometric, low pressure feed conditions used here. It is noted that 0.2 wt.% Rh/SiO_2 showed no measurable methanol conversion under these conditions. E_{app} for AA production was measured to be 155±20 and 133±27 kJ mol^{-1} for 10 wt.% ReO_x/SiO_2 and 0.2 wt.% Rh/10 wt.% ReO_x-SiO_2, respectively (Figure S13). This difference in E_{app} is consistent with the difference in E_{app} for AA production on the 1, 5, and 10 wt.% Re/SiO_2 catalysts, Figure 3a, suggesting Rh may be selectively promoting AA formation on ReO_4 species rather than modifying the inherent barrier. CO preferentially adsorbs on atomically dispersed Rh compared to methanol or methanol-derived intermediates.[70,71] Thus, it is postulated that the formation of $Rh(CO)_2$ species promotes the attempt frequency of CO insertion into neighboring Re-OCH_3 species, although the nature of this interaction deserves further exploration.[22]

4. Discussion and Conclusion

We calculated the volumetric and per metal site reaction rates of AA production on atomically dispersed ReO_4/SiO_2 and Rh-ReO_4/SiO_2 and compared these with other heterogeneous and homogeneous systems (see Table 1). The AA production rates on a per g of metal basis observed for the Re-based catalysts reported here are competitive with Cu modified zeolites,[72,73] atomically dispersed Rh on polymer supports,[13] and atomically dispersed Ir-La site pairs,[11,74] albeit in the absence of high operating pressure, high CO:MeOH feed ratios, and halide co-feeds. The volumetric AA production rates on our Rh-ReO_4/SiO_2 catalyst in a fixed bed process is on par with the Monsanto process and a few-fold lower than the Cavita process.[62]

This comparison demonstrates the substantial potential and operational advantages of the Rh-ReO_4/SiO_2 catalyst reported here. Given that the reaction rates reported here are from measurements at ~30 mbar CO and methanol, and that we observed first order behavior in CO up to 600 mbar partial pressure, it is expected that operating at higher pressure equimolar CO and methanol feeds may significantly further promote the volumetric AA production rates. Further, optimization of the Rh and Re loadings on the basis of volumetric production rate per catalyst cost is likely to enable further optimization of catalyst performance.

Table 1. Comparison with other systems for methanol carbonylation to acetic acid.

* unit conversion from mmol/g/s to mmol/cm^3/s was estimated using catalyst densities and volume fractions.

	Acetic acid production rate	Acetic acid production rate (mmol dm^{-3} s^{-1}) *	CO: methanol molar ratio	Reactor pressure	Reaction temperature	Iodide promotor
10%Re/SiO_2	0.02 mmol g_{Re}^{-1} s^{-1}	0.13	1:1	1 atm	280 °C	-
0.2%Rh/SiO_2	0	0	1:1	1 atm	280 °C	-
0.2%Rh/ 10%Re-SiO_2	0.2 mmol g_{Re}^{-1} s^{-1}	1.3	1:1	1 atm	280 °C	-
1.3%Cu-MOR[26]	0.07 mmol g_{Cu}^{-1} s^{-1}	0.2	200:1	50 atm	270 °C	-
1%Ir-0.7%La/AC[11]	0.15 mmol g_{Ir}^{-1} s^{-1}	1.4	1:1	25 atm	230 °C	CH_3I
2.5%Ni/AC[75]	1.47 mmol g_{Ni}^{-1} s^{-1}	1.8	1:1	11 atm	300 °C	CH_3I
0.265%Rh/ POL-2BPY[13]	3.9 mmol g_{Rh}^{-1} s^{-1}	0.3	1:1	35 atm	Below 200 °C	CH_3I
Monsanto Process (Homogenous)[62,76]		1.5	2:1	30-60 atm	Below 200 °C	HI
Cativa Process (Homogenous)[61]		5.5		28 atm	190 °C	HI

In conclusion, atomically dispersed ReO_4 species on inert SiO_2 supports were observed to be effective heterogeneous methanol carbonylation catalysts without the need for a halide co-feed. The catalytic process exhibited mechanistic similarities to zeolite-based carbonylation catalysts, although the Re-based catalysts promote CO insertion into methoxy species to produce AA, while zeolite catalysts favor methanol insertion into methoxy species prior to carbonylation. Through promotion of the atomically dispersed Re/SiO_2 with atomically dispersed Rh, AA production rates rivaling reports of the Monsanto process were achieved. This work introduces a new class of promising methanol carbonylation catalysts and raises questions about how atomically dispersed pairs sites could act cooperatively to drive catalytic processes.

ASSOCIATED CONTENT

Supporting Information

The Supporting Information is available free of charge online.

EXAFS fitting for Re metal, XANES edge energy for Re standards, calibration curve for Re oxidation state, EXAFS data in k- and R-space, mass transport limitation test, reaction kinetic data, tables for selected mass balance, rate expression derivation, characterization of samples by CO probe molecule FTIR and XPS.

AUTHOR INFORMATION

Corresponding Author
*pchristopher@ucsb.edu

Notes

The authors declare the following competing financial interest(s): J.Q. and P.C. have filed for a patent based on the findings reported in this paper.

ACKNOWLEDGEMENTS

P.C. acknowledges funding from the Air Force Office of Scientific Research MURI Grant FA9550-15-10022. P.C. also acknowledges S. Soled for helpful discussions regarding catalysts synthesis on SiO_2 supports. J.Q. acknowledges funding from the Mellichamp Initiative for Sustainability at the University of California, Santa Barbara. H.R. acknowledges the Postdoctoral Fellowship support by Arnold O. and Mabel Beckman Foundation. The UCSB MRL Shared Experimental Facilities are acknowledged for use of the X-ray Photoelectron Spectroscopy. TEM experiments were conducted using the facilities in the Irvine Materials Research Institute (IMRI) at the University of California-Irvine. Part of this work was also performed at Stanford Synchrotron Radiation Lightsource (SSRL) of SLAC National Accelerator Laboratory and use of the SSRL is supported by the U.S. Department of Energy, Office of Science, Office of Basic Energy Sciences under Contract No. DE-AC02-76SF00515 and by Co-ACCESS supported by the U.S. Department of Energy, Office of Basic Energy Sciences, Chemical Sciences, Geosciences & Biosciences Division.

References

(1) Haynes, A. Catalytic Methanol Carbonylation, 1st ed.; *Elsevier Inc*., **2010**, C, 1-45
(2) Kalck, P.; Le Berre, C.; Serp, P. Recent Advances in the Methanol Carbonylation Reaction into Acetic Acid. *Coord. Chem. Rev*. **2020**, 402, 213078.
(3) Paulik, F. E.; Roth, J. F. Novel Catalysts for the Low-Pressure Carbonylation of Methanol to Acetic Acid. *Chem. Commun*. **1968**, 11 (24), 1578.
(4) Sunley, G. J.; Watson, D. J. High Productivity Methanol Carbonylation Catalysis Using Iridium. The CativaTMprocess for the Manufacture of Acetic Acid. *Catal. Today*. **2000**, 58 (4), 293–307.
(5) Haynes, A. Acetic Acid Synthesis by Catalytic Carbonylation of Methanol. *Top. Organomet. Chem*. **2006**, 18 (5), 179–205.
(6) Ren, Z.; Lyu, Y.; Song, X.; Ding, Y. Review of Heterogeneous Methanol Carbonylation to Acetyl Species. *Appl. Catal. A Gen*. **2020**, 595, 117488.
(7) Howard, M. J.; Jones, M. D.; Roberts, M. S.; Taylor, S. A. C1to Acetyls: Catalysis and Process. *Catal. Today*. **1993**, 18 (4), 325–354.
(8) Hjortkjær, J.; Chen, Y.; Heinrich, B. Methanol Carbonylation in a Liquid Flow System Catalyzed by a Polymer-Bound Rhodium(I) Complex. *Appl. Catal*. **1990**, 67 (1), 269–278.
(9) Feng, S.; Lin, X.; Song, X.; Liu, Y.; Jiang, Z.; Hemberger, P.; Bodi, A.; Ding, Y. The Role of H_2 on the Stability of the Single-Metal-Site Ir_1/AC Catalyst for Heterogeneous Methanol Carbonylation. *J. Catal*. **2020**, 381, 193–203.
(10) Feng, S.; Hemberger, P.; Bodi, A.; Song, X.; Yu, T.; Jiang, Z.; Liu, Y.; Ding, Y. Preparation and Regeneration of Supported Single-Ir-Site Catalysts by Nanoparticle Dispersion via CO and Nascent I Radicals. *J. Catal*. **2020**, 382, 347–357.
(11) Kwak, J. H.; Dagle, R.; Tustin, G. C.; Zoeller, J. R.; Allard, L. F.; Wang, Y. Molecular Active Sites in Heterogeneous Ir-La/C-Catalyzed Carbonylation of Methanol to Acetates. *J. Phys. Chem. Lett*. **2014**, 5 (3), 566–572.
(12) Hensley, A. J. R.; Zhang, J.; Vinçon, I.; Pereira Hernandez, X.; Tranca, D.; Seifert, G.; McEwen, J. S.; Wang, Y. Mechanistic Understanding of Methanol Carbonylation: Interfacing Homogeneous and Heterogeneous Catalysis via Carbon Supported Ir–La. *J. Catal*. **2018**, 361, 414–422.
(13) Ren, Z.; Liu, Y.; Lyu, Y.; Song, X.; Zheng, C.; Feng, S.; Jiang, Z.; Ding, Y. Single-Atom Rh Based Bipyridine Framework Porous Organic Polymer: A High Active and Superb Stable Catalyst for Heterogeneous Methanol Carbonylation. *J. Catal*. **2019**, 369, 249–256.
(14) Ren, Z.; Lyu, Y.; Feng, S.; Song, X.; Ding, Y. A Highly Efficient Single Site Rh-POL-PPh_3 Catalyst for Heterogeneous Methanol Carbonylation. *Mol. Catal*. **2017**, 442, 83–88.
(15) Ren, Z.; Lyu, Y.; Song, X.; Liu, Y.; Jiang, Z.; Lin, R.; Ding, Y. Dual-Ionically Bound Single-Site Rhodium on Porous Ionic Polymer Rivals Commercial Methanol Carbonylation Catalysts. *Adv. Mater.* **2019**, 31 (50), 1–6.
(16) Stepanov, A. G.; Luzgin, M. V.; Romannikov, V. N.; Zamaraev, K. I. NMR Observation of the Koch Reaction in Zeolite H-ZSM-5 under Mild Conditions. *J. Am. Chem. Soc*. **1995**, 117 (12), 3615–3616.
(17) Fujimoto, K.; Shikada, T.; Omata, K.; Tominaga, H. Vapor Phase Carbonylation of Methanol with Solid Acid Catalyst. *Chem. Lett*. **1984**, No. C, 2047–2050.
(18) Bhan, A.; Allian, A. D.; Sunley, G. J.; Law, D. J.; Iglesia, E. Specificity of Sites within Eight-Membered Ring Zeolite Channels for Carbonylation of Methyls to Acetyls. *J. Am. Chem. Soc*. **2007**, 129 (16), 4919–4924.

(19) Sander, S.; Flisch, C.; Geissler, E.; Schoenmakers, H.; Ryll, O.; Hasse, H. Methyl Acetate Hydrolysis in a Reactive Divided Wall Column. *Chem. Eng. Res. Des*. **2007**, 85 (1A), 149–154.
(20) Dingwall, L. D.; Lee, A. F.; Lynam, J. M.; Wilson, K.; Olivi, L.; Deeley, J. M. S.; Gaemers, S.; Sunley, G. J. Bifunctional Organorhodium Solid Acid Catalysts for Methanol Carbonylation. *ACS Catal*. **2012**, 2 (7), 1368–1376.
(21) Blasco, T.; Boronat, M.; Concepción, P.; Corma, A.; Law, D.; Vidal-Moya, J. A. Carbonylation of Methanol on Metal-Acid Zeolites: Evidence for a Mechanism Involving a Multisite Active Center. *Angew. Chemie-Int. Ed*. **2007**, 46 (21), 3938–3941.
(22) Qi, J.; Christopher, P. Atomically Dispersed Rh Active Sites on Oxide Supports with Controlled Acidity for Gas-Phase Halide-Free Methanol Carbonylation to Acetic Acid. *Ind. Eng. Chem. Res.* **2019**, 58 (28), 12632–12641.
(23) Di Iorio, J. R.; Nimlos, C. T.; Gounder, R. Introducing Catalytic Diversity into Single-Site Chabazite Zeolites of Fixed Composition via Synthetic Control of Active Site Proximity. *ACS Catal*. **2017**, 7 (10), 6663–6674.
(24) Di Iorio, J. R.; Hoffman, A. J.; Nimlos, C. T.; Nystrom, S.; Hibbitts, D.; Gounder, R. Mechanistic Origins of the High-Pressure Inhibition of Methanol Dehydration Rates in Small-Pore Acidic Zeolites. *J. Catal*. **2019**, 380, 161-177.
(25) Soled, S. Synthesis of Solid Catalysts. *Wiley-VCH Verlag GmbH & Co. KGaA*. **2009**. Chapter 16.
(26) Corma, A.; Law, D.; Boronat, M.; Martínez-Sánchez, C. Enzyme-like Specificity in Zeolites: A Unique Site Position in Mordenite for Selective Carbonylation of Methanol and Dimethyl Ether with CO. *J. Am. Chem. Soc*. **2008**, 130 (48), 16316–16323.
(27) Boronat, M.; Martínez, C.; Corma, A. Mechanistic Differences between Methanol and Dimethyl Ether Carbonylation in Side Pockets and Large Channels of Mordenite. *Phys. Chem. Chem. Phys.* **2011**, 13 (7), 2603–2612.
(28) Lwin, S.; Keturakis, C.; Handzlik, J.; Sautet, P.; Li, Y.; Frenkel, A. I.; Wachs, I. E. Surface ReO_x Sites on Al_2O_3 and Their Molecular Structure-Reactivity Relationships for Olefin Metathesis. *ACS Catal.* **2015**, 5 (3), 1432–1444.
(29) Barton, D. G.; Shtein, M.; Wilson, R. D.; Soled, S. L.; Iglesia, E. Structure and Electronic Properties of Solid Acids Based on Tungsten Oxide Nanostructures. *J. Phys. Chem. B* **1999**, 103, 630–640.
(30) Hoffman, A. S.; Singh, J. A.; Bent, S. F.; Bare, S. R. In Situ Observation of Phase Changes of a Silica-Supported Cobalt Catalyst for the Fischer-Tropsch Process by the Development of a Synchrotron-Compatible *In Situ/Operando* Powder X-Ray Diffraction Cell. J. Synchrotron Radiat. **2018**, 25 (6), 1673–1682.
(31) Ravel, B.; Newville, M. ATHENA, ARTEMIS, HEPHAESTUS: Data Analysis for X-Ray Absorption Spectroscopy Using IFEFFIT. *J. Synchrotron Radiat*. **2005**, 12 (4), 537–541.
(32) Rehr, J. J.; Albers, R. C.; Zabinsky, S. I. High-Order Multiple-Scattering Calculations of X-Ray-Absorption Fine Structure. *Phys. Rev. Lett*. **1992**, 69 (23), 3397–3400.
(33) Vicente, B. C.; Nelson, R. C.; Moses, A. W.; Chattopadhyay, S.; Scott, S. L. Interactions Involving Lewis Acidic Aluminum Sites in Oxide-Supported Perrhenate Catalysts. *J. Phys. Chem. C* **2011**, 115 (18), 9010–9024.
(34) Bare, S. R.; Kelly, S. D.; D.vila, F.; Boldingh, E.; Karapetrova, E.; Kas, J.; Mickelson, G. E.; Modica, F. S.; Yang, N.; Rehr, J. J. Experimental (XAS, STEM, TPR, and XPS) and Theoretical (DFT) Characterization of Supported Rhenium Catalysts. *J. Phys. Chem. C* **2011**, 115 (13), 5740–5755.

(35) Mishra, R.; Ishikawa, R.; Lupini, A. R.; Pennycook, S. J. Single-Atom Dynamics in Scanning Transmission Electron Microscopy. *MRS Bull*. **2017**, 42 (9), 644–652.
(36) Zhou, W.; Ross-Medgaarden, E. I.; Knowles, W. V.; Wong, M. S.; Wachs, I. E.; Kiely, C. J. Identification of Active Zr-WO_x Clusters on a ZrO_2 Support for Solid Acid Catalysts. *Nat. Chem*. **2009**, 1 (9), 722–728.
(37) She, X.; Kwak, J. H.; Sun, J.; Hu, J.; Hu, M. Y.; Wang, C.; Peden, C. H. F.; Wang, Y. Highly Dispersed and Active ReO_x on Alumina-Modified SBA-15 Silica for 2-Butanol Dehydration. *ACS Catal*. **2012**, 2 (6), 1020–1026.
(38) Resasco, J.; Derita, L.; Dai, S.; Chada, J. P.; Xu, M.; Yan, X.; Finzel, J.; Hanukovich, S.; Hoffman, A. S.; Graham, G. W.; Bare, S. R.; Pan, X.; Christopher, P. Uniformity Is Key in Defining Structure-Function Relationships for Atomically Dispersed Metal Catalysts: The Case of Pt/CeO_2. *J. Am. Chem. Soc*. **2020**, 142 (1), 169–184.
(39) Li, X.; Zhang, B.; Pan, X.; Ji, J.; Ren, Y.; Wang, H.; Ji, N.; Liu, Q.; Li, C. One-Pot Conversion of Lignin into Naphthenes Catalyzed by a Heterogeneous Rhenium Oxide-Modified Iridium Compound. *ChemSusChem*. **2020**, 1–12.
(40) Ma, L.; Li, Y.; He, D. Glycerol Hydrogenolysis to Propanediols over Ru-Re/SiO_2: Acidity of Catalyst and Role of Re. *Chinese J. Catal*. **2011**, 32 (5), 872–876.
(41) Lacheen, H. S.; Cordeiro, P. J.; Iglesia, E. Isolation of Rhenium and ReO_x Species within ZSM-5 Channels and Their Catalytic Function in the Activation of Alkanes and Alkanols. *Chem. - A Eur. J.* **2007**, 13 (11), 3048–3057.
(42) Gallo, A.; Fong, A.; Szeto, K. C.; Rieb, J.; Delevoye, L.; Gauvin, R. M.; Taoufik, M.; Peters, B.; Scott, S. L. Ligand Exchange-Mediated Activation and Stabilization of a Re-Based Olefin Metathesis Catalyst by Chlorinated Alumina. *J. Am. Chem. Soc*. **2016**, 138 (39), 12935–12947.
(43) Zhang, F.; Szeto, K. C.; Taoufik, M.; Delevoye, L.; Gauvin, R. M.; Scott, S. L. Enhanced Metathesis Activity and Stability of Methyltrioxorhenium on a Mostly Amorphous Alumina: Role of the Local Grafting Environment. *J. Am. Chem. Soc*. **2018**, 140 (42), 13854–13868.
(44) Lwin, S.; Keturakis, C.; Handzlik, J.; Sautet, P.; Li, Y.; Frenkel, A. I.; Wachs, I. E. Surface ReO_x sites on Al_2O_3 and Their Molecular Structure-Reactivity Relationships for Olefin Metathesis. *ACS Catal*. **2015**, 5 (3), 1432–1444.
(45) Chauvin, Y.; Commereuc, D. Chemical Counting and Characterization of the Active Sites in the Rhenium Oxide/Alumina Metathesis Catalyst. *J. Chem. Soc. Chem. Commun.* **1992**, 6, 462–464.
(46) Carr, R. T.; Neurock, M.; Iglesia, E. Catalytic Consequences of Acid Strength in the Conversion of Methanol to Dimethyl Ether. *J. Catal*. **2011**, 278 (1), 78–93.
(47) Di Iorio, J. R.; Nimlos, C. T.; Gounder, R. Introducing Catalytic Diversity into Single-Site Chabazite Zeolites of Fixed Composition via Synthetic Control of Active Site Proximity. *ACS Catal*. **2017**, 7 (10), 6663–6674
(48) Cheung, P.; Bhan, A.; Sunley, G. J.; Iglesia, E. Selective Carbonylation of Dimethyl Ether to Methyl Acetate Catalyzed by Acidic Zeolites. *Angew. Chemie-Int. Ed*. **2006**, 45 (10), 1617–1620.
(49) Cheung, P.; Bhan, A.; Sunley, G. J.; Law, D. J.; Iglesia, E. Site Requirements and Elementary Steps in Dimethyl Ether Carbonylation Catalyzed by Acidic Zeolites. *J. Catal*. **2007**, 245 (1), 110–123.
(50) Liu, J.; Zhan, E.; Cai, W.; Li, J.; Shen, W. Methanol Selective Oxidation to Methyl Formate over ReO_x/ CeO_2 Catalysts. *Catal. Lett*. **2008**, 120 (3–4), 274–280.

(51) Clarke, D.B.; Lee, D; Sandoval, M. J.; Bell, A. T. Infrared Studies of the Mechanism of Methanol Decomposition on Cu/SiO_2. *J. Catal*. **1994**, 150, 81-93
(52) Burcham, L. J.; Briand, L. E.; Wachs, I. E. Quantification of Active Sites for the Determination of Methanol Oxidation Turn-over Frequencies Using Methanol Chemisorption and in Situ Infrared Techniques. 1: Supported Metal Oxide Catalysts. *Langmuir* **2001**, 17 (20), 6164–6174.
(53) Zhu, Z.; Espenson, J. H. Organic Reactions Catalyzed by Methylrhenium Trioxide: Dehydration, Amination, and Disproportionation of Alcohols. *J. Org. Chem*. **1996**, 61 (1), 324–328.
(54) Jacob, J.; Espenson, J. H.; Jensen, J. H.; Gordon, M. S. 1,3-Transposition of Allylic Alcohols Catalyzed by Methyltrioxorhenium. *Organometallics* **1998**, 17 (9), 1835–1840.
(55) Korstanje, T. J.; Jastrzebski, J. T. B. H.; Kleingebbink, R. J. M. Mechanistic Insights into the Rhenium-Catalyzed Alcohol-to-Olefin Dehydration Reaction. *Chem.-A Eur. J.* **2013**, 19 (39), 13224–13234.
(56) Christiansen, M. A.; Mpourmpakis, G.; Vlachos, D. G. Density Functional Theory-Computed Mechanisms of Ethylene and Diethyl Ether Formation from Ethanol on γ-Al_2O_3(100). *ACS Catal*. **2013**, 3 (9), 1965–1975.
(57) DeWilde, J. F.; Chiang, H.; Hickman, D. A.; Ho, C. R.; Bhan, A. Kinetics and Mechanism of Ethanol Dehydration on γ-Al_2O_3: The Critical Role of Dimer Inhibition. *ACS Catal*. **2013**, 3 (4), 798–807.
(58) Roy, S.; Mpourmpakis, G.; Hong, D. Y.; Vlachos, D. G.; Bhan, A.; Gorte, R. J. Mechanistic Study of Alcohol Dehydration on γ-Al_2O_3. *ACS Catal*. **2012**, 2 (9), 1846–1853.
(59) Christiansen, M. A.; Mpourmpakis, G.; Vlachos, D. G. DFT-Driven Multi-Site Microkinetic Modeling of Ethanol Conversion to Ethylene and Diethyl Ether on γ-Al_2O_3 (111). *J. Catal*. **2015**, 323, 121–131.
(60) Secordel, X.; Berrier, E.; Capron, M.; Cristol, S.; Paul, J. F.; Fournier, M.; Payen, E. TiO_2-Supported Rhenium Oxide Catalysts for Methanol Oxidation: Effect of Support Texture on the Structure and Reactivity Evidenced by an Operando Raman Study. *Catal. Today* **2010**, 155, 177–183.
(61) Haynes, A.; Maitlis, P. M.; Morris, G. E.; Sunley, G. J.; Adams, H.; Badger, P. W.; Bowers, C. M.; Cook, D. B.; Elliott, P. I. P.; Ghaffar, T.; Green, H.; Griffin, T. R.; Payne, M.; Pearson, J. M.; Taylor, M. J.; Vickers, P. W.; Watt, R. J. Promotion of Iridium-Catalyzed Methanol Carbonylation: Mechanistic Studies of the Cativa Process. *J. Am. Chem. Soc*. **2004**, 126 (9), 2847–2861.
(62) Maitlis, P. M.; Haynes, A.; Sunley, G. J.; Howard, M. J. Methanol Carbonylation Revisited: Thirty Years On. *J. Chem. Soc.-Dalt. Trans*. **1996**, 11, 2187–2196.
(63) Rasmussen, D. B.; Christensen, J. M.; Temel, B.; Studt, F.; Moses, P. G.; Rossmeisl, J.; Riisager, A.; Jensen, A. D. Reaction Mechanism of Dimethyl Ether Carbonylation to Methyl Acetate over Mordenite-a Combined DFT/Experimental Study. *Catal. Sci. Technol*. **2017**, 7 (5), 1141–1152.
(64) Akarmazyan, S. S.; Panagiotopoulou, P.; Kambolis, A.; Papadopoulou, C.; Kondarides, D. I. Methanol Dehydration to Dimethylether over Al_2O_3 catalysts. *Appl. Catal. B Environ*. **2014**, 145, 136–148
(65) Ro, I.; Xu, M.; Graham, G. W.; Pan, X.; Christopher, P. Synthesis of Heteroatom Rh-ReO_x Atomically Dispersed Species on Al_2O_3 and Their Tunable Catalytic Reactivity in Ethylene Hydroformylation. *ACS Catal.* **2019**, 9, 10899–10912.

(66) Yates, J. T.; Kolasinski, K. Infrared Spectroscopic Investigation of the Rhodium Gem-Dicarbonyl Surface Species. *J. Chem. Phys.* **1983**, 79 (2), 1026–1030.
(67) Miessner, H.; Gutschick, D.; Ewald, H.; Miller, H. The Influence of Support on the Geminal Dicarbonyl Species $Rh^{1}(CO)_2$ on Supported Rhodium Catalysts: An IR Spectroscopic Study. *J. Mol. Catal*. **1986**, 36 (1986), 369–373.
(68) Rice, C. A.; Worley, S. D.; Curtis, C. W.; Guin, J. A.; Tarrer, A. R. The Oxidation State of Dispersed Rh on Al_2O_3. *J. Chem. Phys*. **1981**, 74 (11), 6487–6497.
(69) Hoffman, A. S.; Debefve, L. M.; Zhang, S.; Perez-Aguilar, J. E.; Conley, E. T.; Justl, K. R.; Arslan, I.; Dixon, D. A.; Gates, B. C. Beating Heterogeneity of Single-Site Catalysts: MgO-Supported Iridium Complexes. *ACS Catal.* **2018**, 8 (4), 3489–3498.
(70) Tang, Y.; Li, Y.; Fung, V.; Jiang, D. E.; Huang, W.; Zhang, S.; Iwasawa, Y.; Sakata, T.; Nguyen, L.; Zhang, X.; Frenkel, A. I.; Tao, F. Single Rhodium Atoms Anchored in Micropores for Efficient Transformation of Methane under Mild Conditions. *Nat. Commun*. **2018**, 9 (1), 1–11.
(71) Fielicke, A.; Von Helden, G.; Meijer, G.; Pedersen, D. B.; Simard, B.; Rayner, D. M. Size and Charge Effects on the Binding of CO to Small Isolated Rhodium Clusters. *J. Phys. Chem. B* **2004**, 108 (38), 14591–14598.
(72) Yashima, T.; Orikasa, Y.; Takahashi, N.; Hara, N. Vapor Phase Carbonylation of Methanol over RhY Zeolite. *J. Catal.* **1979**, 59 (1), 53–60.
(73) Ni, Y.; Shi, L.; Liu, H.; Zhang, W.; Liu, Y.; Zhu, W.; Liu, Z. A Green Route for Methanol Carbonylation. *Catal. Sci. Technol*. **2017**, 7 (20), 4818–4822.
(74) Ren, Z.; Lyu, Y.; Feng, S.; Song, X.; Ding, Y. Acid-Promoted Ir-La-S/AC-Catalyzed Methanol Carbonylation on Single Atomic Active Sites. *Chinese J. Catal*. **2018**, 39 (6), 1060–1069.
(75) Fujimoto, K.; Omata, K.; Shikada, T.; Tominaga, H. O. Catalytic Features of Carbon Supported Group VIII Metal Catalysts for Methanol Carbonylation. *Prepr. Symp*. **1986**, 31 (1), 85–90.
(76) Nam, J. S.; Rong Kim, A.; Kim, D. M.; Chang, T. S.; Kim, B. S.; Bae, J. W. Novel Heterogeneous Rh-Incorporated Graphitic-Carbon Nitride for Liquid-Phase Carbonylation of Methanol to Acetic Acid. *Catal. Commun*. **2017**, 99 (2), 141–145.

Table of contents image